Diminishing π-Stabilization of an Unsaturated Metal Center: Hydrogen Bonding to OsHCl(CO)(P^tBu_2Me)$_2$

Dmitry V. Yandulov,[†] Kenneth G. Caulton,*[,†] Natalia V. Belkova,[‡] Elena S. Shubina,[‡] Lina M. Epstein,*[,‡] Dmitry V. Khoroshun,[§] Djamaladdin G. Musaev,[§] and Keiji Morokuma*[,§]

Contribution from the Department of Chemistry, Indiana University, Bloomington, Indiana 47405-4001, Institute of Organo-Element Compounds, Russian Academy of Sciences, Vavilov St. 28, Moscow B-334, Russia, and Cherry L. Emerson Center for Scientific Computation and Department of Chemistry, Emory University, Atlanta, Georgia 30322

Received March 6, 1998

Abstract: The interaction between $(CF_3)_2CHOH$ and OsHCl(CO)(P^tBu_2Me)$_2$ in toluene and hexane is shown by ^{1}H NMR (chemical shift, NOE and relaxation times) and IR (ν_{CO}, ν_{Os-H}, and ν_{Os-Cl}) spectroscopies to involve $-\Delta H^\circ \approx 3-4$ kcal/mol and $-\Delta S^\circ \approx 7-9$ cal mol^{-1} K^{-1}. Integrated molecular orbital/molecular mechanics calculations show definitively that the hydrogen bond acceptor is chloride and that steric effects preclude any O→Os donation by the alcohol. Analysis of the calculated energies and structures shows that such hydrogen bonding increases the electrophilic character of the unsaturated osmium.

Introduction

Of paramount importance in biological and organic chemistry,[1] hydrogen bonding has attracted much attention in the chemistry of transition metals. A number of potential donor and acceptor sites have been identified for metal complexes in the solid state. Remote acidic C−H,[2a] N−H,[2b], and O−H[2c,d] moieties of the ligands as well as directly coordinated hydroxyl,[2e,f] amine,[2g] ammine,[2h] and hydride[2i−l] ligands can donate hydrogen bonds, while accepting counterparts can be as diverse as halide,[3a−e] pseudohalide,[3f,h] carbonyl,[2a] hydride,[3i,2k] or aromatic[3j] ligands and even the metal[3k−m,2k] itself. The resulting multitude of possible bonding patterns has been utilized in applying the principles of molecular recognition, based on complementary hydrogen bonding, in crystal engineering of transition metal organo networks.[4]

Regular hydrogen bonding is a weak ($\Delta H^\circ \leq 15$ kcal mol^{-1}) interaction. In solution most of the above types of bonding are retained predominantly in intramolecular cases,[3e,i,5] while the larger ΔS° causes intermolecular hydrogen bonded aggregates to be present in dynamic equilibrium with free constituents at ambient temperatures.[6−10] In the latter case, hydrogen bonding equilibrium may be further complicated by competition between several viable hydrogen bond acceptors in the same molecule.[3j,7,8,10,11] Knowledge of the preferred accepting site is fundamental to understanding the electronic structure of the complex in question and our predictive ability is currently inadequate.

Due to its small interaction enthalpy, hydrogen bonding generally results only in a small perturbation of the electronic

[†] Indiana University.

[‡] Russian Academy of Sciences.

[§] Emory University.

(1) Jeffrey G. A.; Saenger, W. *Hydrogen Bonding in Biological Structures*; Springer: Berlin, 1991.

(2) (a) Braga, D.; Grepioni, F.; Biradha, K.; Pedireddi, V. R.; Desiraju, G. R. *J. Am. Chem. Soc.* **1995**, *117*, 3156. (b) Batsanov, A. S.; Hubberstey, P.; Russel, C. E. *J. Chem. Soc., Dalton Trans.* **1994**, 3189. (c) Braga, D.; Grepioni, F.; Sabatino, P.; Desiraju, G. R. *Organometallics* **1994**, *13*, 3532. (d) Stevens, R. C.; Bau, R.; Milstein, D.; Blum, O.; Koetzle, T. F. *J. Chem. Soc., Dalton Trans.* **1990**, 1429. (e) Canty, A. J.; Jin, H.; Skelton, B. W.; White, A. H. *J. Organomet. Chem.* **1995**, *503*, C16. (f) Winter, C. H.; Sheridan, P. H.; Heeg, M. J. *Inorg. Chem.* **1991**, *30*, 1962. (g) Brammer, L.; Charnock, J. M.; Goggin, P. L.; Goodfellow, R. J.; Orpen, A. G.; Koetzle, T. F. *J. Chem. Soc., Dalton Trans.* **1991**, 1789. (h) Figgis, B. N.; Kucharski, E. S.; Vrtis, M. *J. Am. Chem. Soc.* **1993**, *115*, 176. (i) Braga, D.; Grepioni, F.; Tedesco, E.; Biradha, K.; Desiraju, G. R. *Organometallics* **1996**, *15*, 2692. (j) Peris, E.; Crabtree, R. H. *J. Chem. Soc., Chem. Commun.* **1995**, 2179. (k) Shubina, E. S.; Belkova, N. V.; Epstein, L. M. *J. Organomet. Chem.* **1997**, *536*, 17. (l) Epstein, L. M.; Shubina, E. S.; Krylov, A. N.; Kreindlin, A. Z.; Rybinskaya, M. I. *J. Organomet. Chem.* **1993**, *447*, 2771.

(3) (a) Murphy, V. J.; Hascall, T.; Chen, J. Y.; Parkin, G. *J. Am. Chem. Soc.* **1996**, *118*, 7428. (b) Richmond, T. G. *Coord. Chem. Rev.* **1990**, *105*, 221. (c) Davies, P. J.; Veldman, N.; Grove, D. M.; Spek, A. L.; Lutz, B. T. G.; van Koten, G. *Angew. Chem., Int. Ed. Engl.* **1996**, *35*, 1959. (d) Yap, G. P. A.; Rheingold, A. L.; Das, P.; Crabtree, R. H. *Inorg. Chem.* **1995**, *34*, 3474. (e) Fryzuk, M. D.; MacNeil, P. A.; Rettig, S. J. *J. Am. Chem. Soc.* **1987**, *109*, 2803. (f) Kim, Y. J.; Osakada, K.; Takenaka, A.; Yamamoto, A. *J. Am. Chem. Soc.* **1990**, *112*, 1096. (g) Kegley, S. E.; Schaverien, C. J.; Freudenberger, J. H.; Bergman, R. G.; Nolan, S. P.; Hoff, C. D. *J. Am. Chem. Soc.* **1987**, *109*, 6563. (h) Alsters, P. L.; Baesjou, P. J.; Janssen, M. D.; Kooijman, H.; Sicherer-Roetman, A.; Spek, A. L.; van Koten, G. *Organometallics* **1992**, *11*, 4124. (i) Crabtree, R. H.; Siegbahn, P. E. M.; Eisenstein, O.; Rheingold, A. L. *Acc. Chem. Res.* **1996**, *29*, 348. (j) Epstein, L. M.; Krylov, A. N.; Shubina, E. S. *J. Mol. Struct.* **1994**, *322*, 345. (k) Brammer, L.; Zhao, D.; Lapido, F. T.; Braddock-Wilking, J. *Acta Crystallogr.* **1995**, *B51*, 632. (l) Yao, W.; Eisenstein, O.; Crabtree, R. H. *Inorg. Chim. Acta* **1997**, *254*, 105. (m) Braga, D.; Grepioni, F.; Tedesco, E.; Biradha, K.; Desiraju, G. R. *Organometallics* **1997**, *16*, 1846.

(4) Burrows, A. D.; Chan, C. W.; Chowdhry, M. M.; McGrady, J. E.; Mingos, D. M. P. *Chem. Soc. Rev.* **1995**, *24*, 329.

(5) (a) Epstein, L. M.; Shubina, E. S. *Organomet. Chem. USSR* **1992**, *5*, 31. (b) Fairhurst, S. A.; Henderson, R. A.; Hughes, D. L.; Ibrahim, S. K.; Pickett, C. J. *J. Chem. Soc., Chem. Commun.* **1995**, 1569.

(6) Shubina, E. S.; Belkova, N. V.; Krylov, A. N.; Vorontsov, E. V.; Epstein, L. M.; Gusev, D. G.; Niedermann, M.; Berke, H. *J. Am. Chem. Soc.* **1996**, *118*, 1105.

(7) Belkova, N. V.; Shubina, E. S.; Ionidis, A. V.; Epstein, L. M.; Jacobsen, H.; Messmer, A.; Berke, H. *Inorg. Chem.* **1997**, *36*, 1522.

(8) Kazarian, S. G.; Hamley, P. A.; Poliakoff, M. *J. Am. Chem. Soc.* **1993**, *115*, 9069.

(9) Hamley, P. A.; Kazarian, S. G.; Poliakoff, M. *Organometallics* **1994**, *13*, 1767.

(10) Shubina, E. S.; Krylov, A. N.; Kreindlin, A. Z.; Rybinskaya, M. I.; Epstein, L. M. *J. Mol. Struct.* **1993**, *301*, 1.

(11) Epstein, L. M.; Krylov, A. N.; Shubina, E. S.; Borisov, A. P.; Makhaev, V. D. *Int. Conf. Organomet. Chem., XIVth* **1994**, 313.

10.1021/ja980751p CCC: $15.00
Published on Web 11/17/1998

structures of the participating molecules. Nakamura[12a] and Walters[12b,c] have shown NH···S intramolecular interactions to be responsible for positive shifts of redox potentials of several molybdenum thiolates as models for cysteine−metal electron-transfer proteins. Lappin et al. have found[12d] NH···O intermolecular hydrogen bonds to facilitate electron-transfer reactions of $[Co(en)_3]^{2,3+}$, and Bruno and co-workers suggested[12e] ROH···O bonding to limit the reduction of $[Cp'_2Nb(\eta^2\text{-}CH_2O)]^{\bullet}$. Highly pertinent to homogeneous catalysis, Braunstein and co-workers have shown how intramolecular hydrogen bonding to the oxygen atom of an η^2-(P,O)-diphenylphosphinoenolate ligand in a nickel SHOP catalyst can determine molecular weight distribution of the products.[12f] It appears that hydrogen bonding offers a unique opportunity to fine-tune the necessary electronic properties of a complex.

The formally unsaturated 16-electron complex $OsHCl(CO)(P^tBu_2Me)_2$ (**1**)[13a] is representative of the broad class of compounds of general formula $MHX(CO)P_2$ (M = Ru, Os;[13b] X = halide, pseudohalide;[14] P = P^tBu_2Me,[13c] P^iPr_3[13b]) that adopt nearly square-pyramidal geometry with apical hydride and *trans*-disposed bulky phosphines, preventing aggregation via halide bridging,[13b] and are stabilized via "push−pull" interactions between the filled X ligand π, metal d_π, and vacant CO π^* orbitals.[14] Although such stabilization results in partial delocalization of the π-density of the X ligand into the π^* orbitals of the carbonyl ligand, the X ligand may retain significant nucleophilic character. For example, the fluoride ligand of $RuHF(CO)(P^tBu_2Me)_2$ was found to accept a hydrogen bond from methanol in solution.[14c] The complexes of the above composition exhibit a wide range of reactivity,[14b,15] while $OsHCl(CO)(P^iPr_3)_2$ is an effective catalyst for hydrogenation and hydrosilylation of unsaturated organic substrates.[16]

We report here on hydrogen bonding between **1** and a sufficiently strong hydrogen bond donor investigated to find (1) the preferred accepting site and (2) how and to what extent the electronic structure of the complex can be modified via intermolecular hydrogen bonding.

Results

I. NMR Study of the Interaction between $OsHCl(CO)(P^tBu_2Me)_2$ and $(CF_3)_2CHOH$ (HFIP). (a) Evidence for Interaction.

Increasing the mole ratio of [HFIP°] to [**1**°] in d_8-toluene solution from 0.5 to 5 and/or decreasing the temperature from 20 to −90 °C resulted in a gradual upfield shift of the hydride resonance of **1**, as shown in Figure 1. The maximum observed shift of 1.36 ppm is well beyond the experimental error and is unlikely to be due to self-association of **1** via chloride ligand bridging or coordination of the alcohol oxygen to the metal. The large body of accumulated empirical evidence[13b,14c,16a−c] shows that coordination of a Lewis base *trans* to a hydride ligand generally causes a significant *downfield* shift of its resonance.

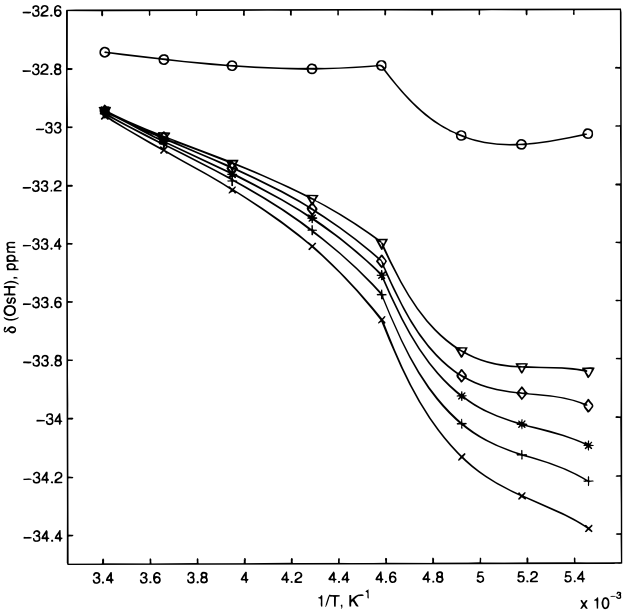

Figure 1. Variable-temperature hydride chemical shifts in $OsHCl(CO)(P^tBu_2Me)_2$ (**1**)/HFIP in d_8-toluene. For temperatures below −55 °C ($1/T = 4.6 \times 10^{-3}$ K^{-1}) the values shown correspond to those of the symmetric (M_2) rotamer (see text for details). The [**1**°]/[HFIP°] concentrations are 11.4/57.0 (×), 38.0/57.0 (+), 57.0/57.0 (∗), 85.5/57.0 (◊), 114.0/57.0 (▽), and 11.4/;0 (○) mmol L^{-1}, respectively.

The steric bulk of the phosphines in **1**, P^tBu_2Me (cone angle 161°), is manifested in hindered rotation[17] about Os−P bonds. By −100 °C, the $^{31}P\{^1H\}$ NMR spectrum of pure **1** in d_8-toluene consists of one AB (J_{PP} = 258 Hz) and one M_2 pattern, corresponding to two frozen rotamers, and two corresponding hydride signals are observed by ^1H NMR. Figure 2 shows that the frozen conformations of **1** are quite sensitive to the presence of HFIP. Both the hydride and ^{31}P NMR signals shift upfield, while integration of the hydride signals reveals a steady decrease in the [AB]/[M_2] mole ratio from 0.32 to 0.21, corresponding to the increase of the [HFIP°]/[**1**°] from 0 to 5. The ^1H NMR spectra reveal another, more subtle feature: while no multiplet structure is resolved in the M_2 hydride signal at −90 °C, increasing [HFIP°]/[**1**°] leads to gradual sharpening of the resonance at this temperature into a triplet ($^2J_{PH}$). This sharpening indicates that HFIP additionally hinders the rotation around Os−P bonds in **1**, consistent with adduct formation.

Spin−lattice relaxation rates of the hydride resonance of **1**, dominated[18] by dipolar coupling to the phosphine protons,[19] show little change in the presence of HFIP (Figure 3). Such

(12) (a) Ueyama, N.; Okamura, T. A.; Nakamura, A. *J. Am. Chem. Soc.* **1992**, *114*, 8129. (b) Huang, J.; Ostrander, R. L.; Rheingold, A. L.; Leung, Y. C.; Walters, M. A. *J. Am. Chem. Soc.* **1994**, *116*, 6769. (c) Huang, J. O.; Ostrander, R. L.; Rheingold, A. L.; Walters, M. A. *Inorg. Chem.* **1995**, *34*, 1090. (d) Warren, R. M. L.; Tatehata, A.; Lappin, A. G. *Inorg. Chem.* **1993**, *32*, 1191. (e) Thiyagarajan, B.; Michalczyk, L.; Bollinger, J. C.; Huffman, J. C.; Bruno, J. W. *Organometallics* **1996**, *15*, 1989. (f) Braunstein, P.; Chauvin, Y.; Mercier, S.; Saussine, L.; De Cian, A.; Fischer, J. *J. Chem. Soc., Chem. Commun.* **1994**, 2203.

(13) (a) Werner, H.; Esteruelas, M. A.; Meyer, U.; Wrackmeyer, B. *Chem. Ber.* **1987**, *120*, 11. (b) Esteruelas, M. A.; Werner, H. *J. Organomet. Chem.* **1986**, *303*, 221. (c) Gill, D. F.; Shaw, B. L. *Inorg. Chim. Acta* **1979**, *32*, 19.

(14) (a) Poulton, J. T.; Folting, K.; Streib, W. E.; Caulton, K. G. *Inorg. Chem.* **1992**, *31*, 3190. (b) Poulton, J. T.; Sigalas, M. P.; Eisenstein, O.; Caulton, K. G. *Inorg. Chem.* **1993**, *32*, 5490. (c) Poulton, J. T.; Sigalas, M. P.; Folting, K.; Streib, W. E.; Eisenstein, O.; Caulton, K. G. *Inorg. Chem.* **1994**, *33*, 1476.

(15) Bourgault, M.; Castillo, A.; Esteruelas, M. A.; Oñate, E.; Ruiz, N. *Organometallics* **1997**, *16*, 636 and references therein.

(16) (a) Esteruelas, M. A.; Sola, E.; Oro, L. A.; Meyer, U.; Werner, H. *Angew. Chem., Int. Ed. Engl.* **1988**, *27*, 1563. (b) Andriollo, A.; Esteruelas, M. A.; Meyer, U.; Oro, L. A.; Sánchez-Delgado, R. A.; Sola, E.; Valero, C.; Werner, H. *J. Am. Chem. Soc.* **1989**, *111*, 7431. (c) Esteruelas, M. A.; Valero, C.; Oro, L. A.; Meyer, U.; Werner, H. *Inorg. Chem.* **1991**, *30*, 1159. (d) Esteruelas, M. A.; Oro, L. A.; Valero, C. *Organometallics* **1991**, *10*, 462. (e) Esteruelas, M. A.; Oro, L. A.; Valero, C. *Organometallics* **1992**, *11*, 3362. (f) Bakhmutov, V. I.; Bertrán, J.; Esteruelas, M. A.; Lledós, A.; Maseras, F.; Modrego, J.; Oro, L. A.; Sola, E. *Chem. Eur. J.* **1996**, *2*, 815.

(17) Notheis, J. U.; Heyn, R. H.; Caulton, K. G. *Inorg. Chim. Acta* **1995**, *229*, 187 and references therein.

(18) Gusev, D. G.; Kuhlman, R. L.; Renkema, K. B.; Eisenstein, O.; Caulton, K. G. *Inorg. Chem.* **1996**, *35*, 6775.

(19) Desrosiers, P. J.; Cai, L.; Lin, Z.; Richards, R.; Halpern, J. *J. Am. Chem. Soc.* **1991**, *113*, 4173.

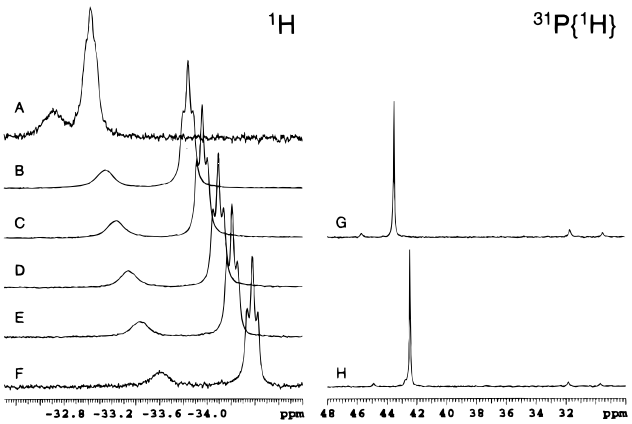

Figure 2. 300 MHz ^{1}H NMR (hydride region, −90 °C) (left) and 122 MHz ^{31}P{^{1}H} NMR (−100 °C) (right) spectra of OsHCl(CO)(P^{t}Bu$_2$Me)$_2$ (**1**)/HFIP in d_8-toluene. The [**1**°]/[HFIP°] concentrations are 11.4/0 (A), 114.0/57.0 (B), 85.5/57.0 (C), 57.0/57.0 (D), 38.0/57.0 (E), 11.4/57.0 (F), 11.4/0 (G), and 19.0/57.0 (H) mmol L^{-1}, respectively.

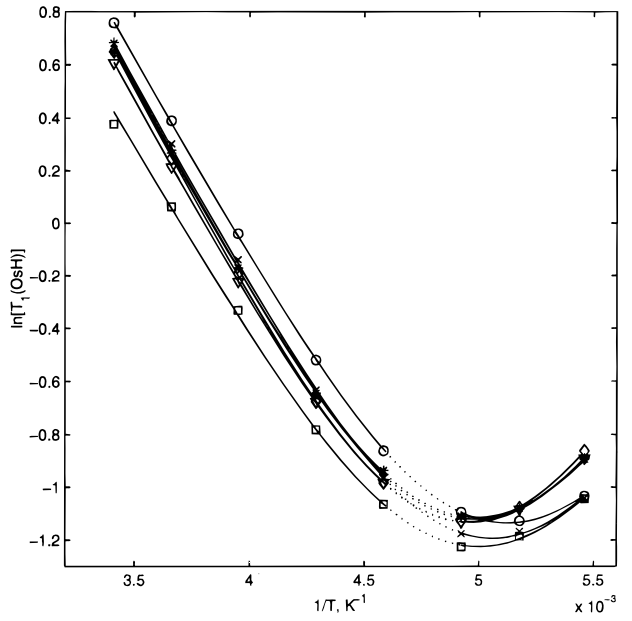

Figure 3. Variable-temperature spin−lattice relaxation times of the hydride ligand in OsHCl(CO)(P^{t}Bu$_2$Me)$_2$ (**1**)/HFIP in d_8-toluene. For temperatures below −55 °C ($1/T = 4.6 \times 10^{-3}$ K^{-1}) the values shown correspond to those of the symmetric (M_2) rotamer (see text for details). The [**1**°]/[HFIP°] concentrations are 11.4/57.0 (×), 38.0/57.0 (+), 57.0/57.0 (∗), 85.5/57.0 (◊), 114.0/57.0 (▽), and 11.4/0 (○) mmol L^{-1}, respectively. Values calculated for the fully formed adduct **1′** are shown with (□).

behavior is very different from the significantly reduced $T_{1\min}$ values when hydrogen bonding occurs to the hydride ligand itself.[3i,6] The maximum observed decrease of the hydride $T_{1\min}$ from 321 to 303 ms is close to the experimental error, although the temperature profiles show that the presence of HFIP slightly shifts the minima to higher temperatures. Analogous, but smaller changes are observed in spin−lattice relaxation times of the phosphine protons and are indicative of an effective increase of the complex size[19] in agreement with adduct formation.

More dramatic changes are observed for the ^{1}H NMR resonances of HFIP as the amount of [**1**°] present is varied (Figure 4). An undesirable characteristic of an alcohol as acidic as HFIP is its high sensitivity to adventitious impurities. In the present case, traces (<5 mol %) of water present in **1** from

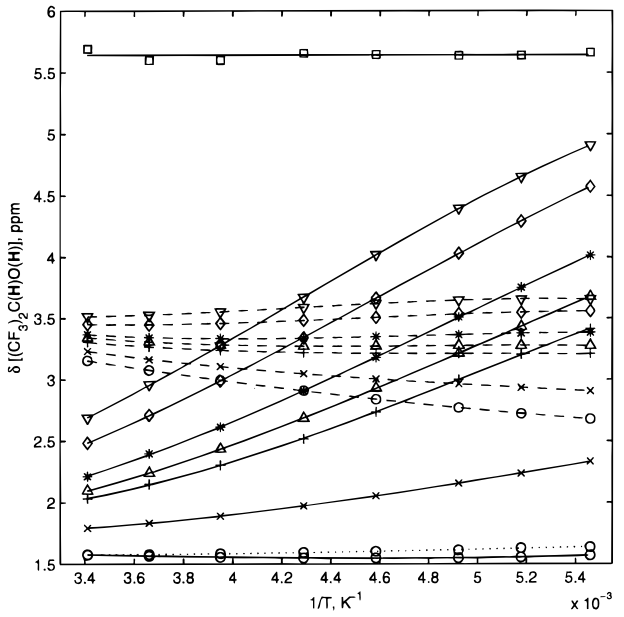

Figure 4. Variable-temperature chemical shifts of OH (−) and CH (- - -) resonances of HFIP in the presence of variable amounts of OsHCl(CO)(P^{t}Bu$_2$Me)$_2$ (**1**) in d_8-toluene. The [HFIP°]/[**1**°] concentrations are 57.0/0 (○), 57.0/11.4 (×), 57.0/38.0 (+), 57.0/45.6 (△), 57.0/57.0 (∗), 57.0/85.5 (◊), and 57.0/114.0 (▽) mmol L^{-1}, respectively. The dotted line connects the OH chemical shifts in pure HFIP in the presence of water. Shown with (□) are the calculated OH chemical shifts in the adduct **1′**. See text for details.

its synthesis[13a] cause fast intermolecular exchange of the hydroxyl proton, averaging out the CH−OH coupling of $^3J_{HH}$ = 8.5 Hz. However, the effect water has on the OH chemical shift is small. Shown with a dotted line in Figure 4 is the temperature dependence of the OH chemical shift in a d_8-toluene solution of HFIP with approximately the maximum water content, present in experiments with **1**. The deviation from the OH chemical shift in a dry solution does not exceed 0.16 ppm, which, compared to the shifts of [0.22−4.34] ppm observed in the presence of **1** (Figure 4), allow the latter shifts to be attributed predominantly to an interaction of HFIP with **1**. Nevertheless, the presence of water significantly increases[20] spin−lattice relaxation rates of both OH and CH protons, making the T_1 measurements for both CH and OH signals of no practical use, because the effect is very sensitive to the exact water concentration.

Moderate NOE's were observed between the phosphine protons of **1** and those of HFIP (OH, CH) at [**1**°] = 21.7 and [HFIP°] = 65.2 mmol L^{-1} in a series of experiments at 20, −40, and −90 °C and were found to be maximum by absolute magnitude at the lowest temperature. At −90 °C, irradiation of either methyl or *tert*-butyl resonances of **1** led to 25% and 15% decreases in OH and CH signal intensities, respectively, while irradiation of the OH resonance gave negative NOE's of 6% for the methyl and 3% for the *tert*-butyl signals. While the magnitude of the latter effect is close to the limit of error (estimated ≤2%), other NOE's are sufficiently strong and indicate the presence of the OH proton in proximity to the phosphine alkyl groups, consistent with hydrogen-bonded adduct formation. Since operation of a *negative* NOE regime was

(20) (a) The most likely operating mechanisms are scalar relaxation of the first kind via modulation of CH−OH scalar coupling[20b] and proton−proton dipole−dipole interactions[19] in any plausible hydrogen-bonded adducts of HFIP with water. (b) Abragam, A. *The Principles of Nuclear Magnetism*; Oxford University Press: London, 1961.

Table 1. Equilibrium Constants for Formation of Adduct **1′** (K) (see Eq 1)

T, K	293	273	253	233	218	203	193	183
K, L mol^{-1}	3.81(7)[a]	5.67(7)	8.34(8)	12.7(1)	19.1(2)	30.8(3)	44.1(8)	65(1)

[a] Standard deviations are given in parentheses.

evident from observation of negative effects between essentially every pair of protons, the negative NOE's of 2−3% measured for phosphine protons on irradiation of CH and for OH and OsH on irradiation of OsH and OH, respectively, are likely to be due to spin diffusion rather than a direct interaction,[21] if reliable at all. The weakness of the OsH NOE induced by irradiation of OH is consistent with the results of hydride T_1 measurements (*vide supra*). For comparison,[6] the direct $(CF_3)_2$-CHOH···HW(CO)$_2$(NO)(PMe$_3$)$_2$ intermolecular interaction was found to give 26% negative NOE for the hydride signal upon irradiation of the hydroxyl resonance, while irradiation of WH reduced the signal intensity of OH by 10% at −90 °C.

(b) Thermodynamics of the Hydrogen Bonding. The experimental data present considerable evidence for intermolecular interaction between HFIP and **1** in solution. The significant downfield shift of the OH resonance is characteristic of hydrogen bonding,[1] while the presence of the alcohol in the *first* solvation sphere of the osmium complex is manifested in the NOE data as well as by increased hindrance of rotation about the Os−P bonds. The downfield shift of the CH signal is likely to be due to interaction of HFIP with **1** via the OH group precluding the methine proton from hydrogen bonding with the aromatic ring of the solvent, d_8-toluene, for steric reasons. Assuming that a 1:1 adduct (**1′**) is reversibly formed in solution (eq 1), one can relate[22] the unknown equilibrium constant, *K*,

$$\underset{\mathbf{1}}{\mathrm{OsHCl(CO)(P^tBu_2Me)_2}} + (CF_3)_2CHOH \overset{K}{\rightleftharpoons} \underset{\mathbf{1'}}{[(CF_3)_2CHOH]\cdots[OsHCl(CO)(P^tBu_2Me)_2]} \quad (1)$$

to the observed averaged chemical shift of (the most sensitive) hydroxyl proton (δ^{OH}_{obs}) via the other unknown, chemical shift in the adduct **1′** (δ^{OH}_b):

$$K(\delta^{OH}_b) = \frac{\delta^{OH}_{obs} - \delta^{OH}_f}{(\delta^{OH}_b - \delta^{OH}_{obs})\left([\mathbf{1}^\circ] - \dfrac{(\delta^{OH}_{obs} - \delta^{OH}_f)[\mathrm{HFIP}^\circ]}{\delta^{OH}_b - \delta^{OH}_f}\right)}$$

where [**1**°] and [HFIP°] are the total concentrations and δ^{OH}_f is the OH chemical shift in the free alcohol. With use of the averaged OH chemical shift at the five highest [**1**°] concentrations (Figure 4), the resulting series of simultaneous equations was fitted[23] at eight temperatures to yield the equilibrium constants (Table 1) and essentially constant $\delta^{OH}_b = 5.64 \pm 0.05$ ppm, also shown in Figure 4. The temperature dependence of the obtained equilibrium constants (Figure 5) was analyzed to give $\Delta H° = -2.7(1)$ kcal mol^{-1} and $\Delta S° = -6.6(5)$ cal mol^{-1} K^{-1} for the formation of **1′**. The obtained $\Delta S°$ value is less negative than might be expected for eq 1, which decreases the number of particles. Together with the unusually high field and temperature-independent OH chemical shift of pure HFIP

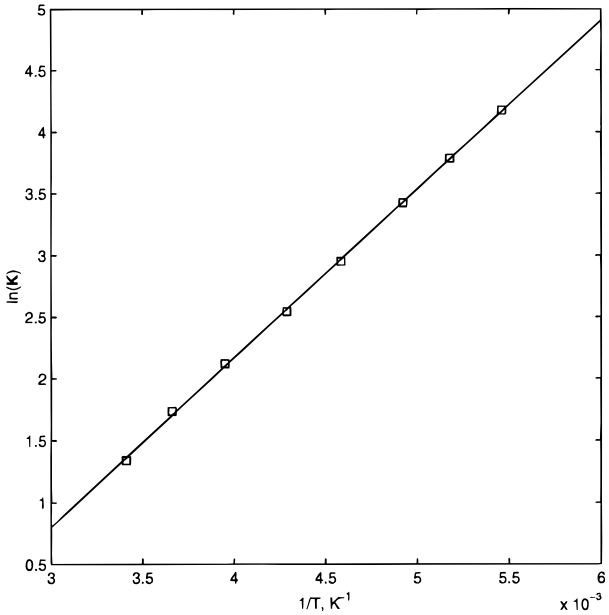

Figure 5. van't Hoff plot of the equilibrium constants for formation of adduct **1′**.

(Figure 4) this suggests that "free" HFIP in eq 1 hydrogen bonds to toluene.[24] Using the values of δ^{OH}_f measured in the presence of water in the analysis gives the values of $\Delta H°$ and $\Delta S°$ that are within the error bounds on the values given above, although the discrepancy of the δ^{OH}_b and *K* values is much greater.

(c) Structural Implications. The alcohol molecule is definitely present in the first solvation sphere of the osmium, as follows from the NOE data and the additional hindrance of rotation about the Os−P bonds. The downfield shift of the hydroxyl proton resonance assures that the hydroxyl group acts as a hydrogen bond donor,[1] while the upfield shift of the hydride signal indicates no significant coordination of HFIP to the osmium through the oxygen lone pair (*vide supra*). This lack of O→Os donation is consistent with the electron-withdrawing influence of the $(CF_3)_2CH$ group on oxygen basicity, as well as steric effects of $(CF_3)_2CH$ and P^{t}Bu$_2$Me.

The T_{1min} data of the hydride signal unambiguously exclude the hydride as the hydrogen bond accepting site in **1**. The presence of the hydroxyl proton at the longest conceivable OH···HOs hydrogen bond distance of ≤2.5 Å would increase the spin−lattice relaxation rate R_{1max} ($=1/T_{1min}$) of the hydride by $R_{1max} \geq 129.21/(2.5)^6 = 0.53$ s^{-1} (at 300 MHz),[19] giving T_{1min} of the hydride in **1′** as $T_{1min} \leq (1/T_{1min}(\mathbf{1}) + 0.53)^{-1} = (1/0.321 + 0.53)^{-1} =$ **274** ms. By using the obtained equilibrium constants and the measured hydride T_1 times in pure **1** and in

(21) Neuhaus, D.; Williamson, M. P. *The Nuclear Overhauser Effect in Structural and Conformational Analysis*; VCH Publishers: New York, 1989.
(22) Drago, R. S. *Physical Methods for Chemists*; Saunders College Publishing: Orlando, 1992; p 291.
(23) Slejko, F. L.; Drago, R. S.; Brown, D. G. *J. Am. Chem. Soc.* **1972**, *94*, 9210.
(24) (a) Yoshida, Z.; Ōsawa, E. *J. Am. Chem. Soc.* **1965**, *87*, 1467. (b) Yoshida, Z.; Ōsawa, E. *J. Am. Chem. Soc.* **1966**, *88*, 4019. (c) Gramstad, T.; Simonsen, O. R. *Spectrochim. Acta* **1976**, *32A*, 723. (d) Al-Imarah, F. J. M.; Kamounah, F. S.; Salman, S. R. *Spectrosc. Lett.* **1990**, *23*, 545. (e) Cheney, B. V.; Schulz, M. W.; Cheney, J.; Richards, W. G. *J. Am. Chem. Soc.* **1988**, *110*, 4195. (f) West, R.; Powell, D. L.; Lee, M. K. T.; Whatley, L. S. *J. Am. Chem. Soc.* **1964**, *86*, 3227. (g) West, R.; Whatley, L. S.; Lake, K. J. *J. Am. Chem. Soc.* **1961**, *83*, 761. (h) Johnson, C. E.; Bovey, F. A. *J. Chem. Phys.* **1958**, *29*, 1012. (i) Suzuki, S.; Green, P. G.; Bumgarner, R. E.; Dasgupta, S.; Goddard, W. A., III; Blake, G. A. *Science* **1992**, *257*, 942.

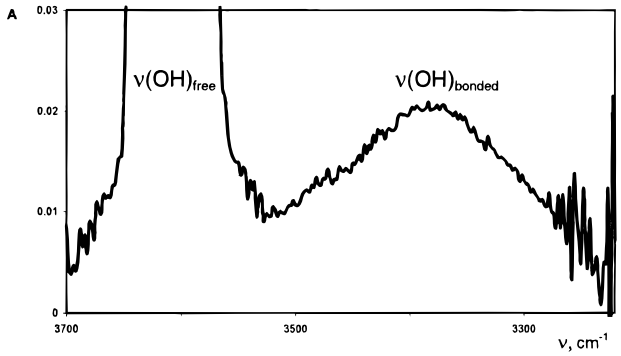

Figure 6. IR spectrum of HFIP (ν(OH) region, 20 °C) in the presence of OsHCl(CO)(P^{t}Bu$_2$Me)$_2$ (**1**) in hexane. The [**1**°]/[HFIP°] concentrations are 5.0/1.0 mmol L^{-1}, respectively.

Table 2. ν(OH) Data of TFE and HFIP in the Presence of OsHCl(CO)(P^{t}Bu$_2$Me)$_2$ (**1**) in Hexane

ROH	ν(OH)$_{free}$, cm^{-1}	ν(OH)$_{bonded}$, cm^{-1}	$\Delta\nu$(OH),[a] cm^{-1}	$-\Delta$H°, kcal mol^{-1}
TFE	3632	3450	182	3.6
HFIP	3611[b]	3388	223	4.3

[a] $\Delta\nu$(OH) = ν(OH)$_{free}$ − ν(OH)$_{bonded}$. [b] For HFIP, the frequency ν(OH)$_{free}$ was determined as the mean of 3631 and 3592 cm^{-1}.

the presence of 5 equiv of HFIP, the actual T_{1min} of the hydride in **1′** is calculated as **294** ms (Figure 3), which is detectably longer than the estimated value. The observed (small) decrease of the hydride T_1 is likely to be due to hydrogen bonding with HFIP increasing the steric repulsion of the phosphines, which bend more toward the smallest ligand, the hydride, and increase dipolar interactions with the alkyl protons.

In summary, the NMR data restrict the position of the HFIP in **1′** to the side opposite to the hydride ligand and show any O→Os interaction to be close to nonexistent. To further elucidate the nature of the hydrogen bonding between **1** and HFIP, IR studies were undertaken.

II. IR Investigation of Hydrogen Bonding between OsHCl(CO)(P^{t}Bu$_2$Me)$_2$ and Acidic Alcohols. (a) Evidence for Interaction. Fluorinated alcohols CF_3CH_2OH (TFE) and $(CF_3)_2CHOH$ (HFIP) in the presence of **1** in hexane show a typical pattern in the region of O−H stretching vibrations, characteristic of hydrogen bonding.[6,7] The ν(OH) bands of the free alcohols decrease in intensity, while new broad bands appear at lower frequencies (Figure 6). As shown in Table 2, the magnitude of the shift increases with the proton-donating ability of the alcohol (TFE < HFIP). By using the measured ν(OH) values, enthalpies of the hydrogen bonds with TFE and HFIP were calculated by empirical eq 2[25] (Table 2).

$$-\Delta H^\circ = \frac{18\Delta\nu(\mathrm{OH})}{\Delta\nu(\mathrm{OH}) + 720} \qquad (2)$$

The applicability of eq 2, initially developed for hydrogen bonds with organic bases, to hydrogen bonded systems with organometallic bases has been shown previously.[6,26] It is noteworthy that no low-frequency hydrogen-bonded O−H bands were observed with the weaker proton donors, methanol or 2-propanol.

(b) Effect on the Metal Complex. The IR spectrum of **1** shows a ν(CO) band at 1889 cm^{-1} and a broad ($\Delta\nu_{1/2}$ = 20 cm^{-1}) ν(OsH) band at 1948 cm^{-1} that are essentially constant

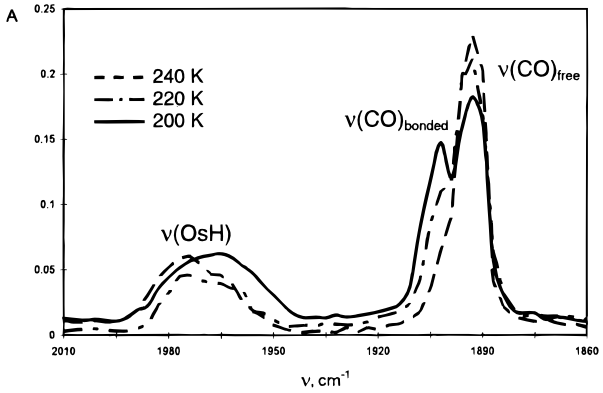

Figure 7. Variable-temperature IR spectra (ν(OsH) and ν(CO) regions) of OsHCl(CO)(P^{t}Bu$_2$Me)$_2$ (**1**) in the presence of HFIP in hexane. The [**1**°]/[HFIP°] concentrations are 1.0/10.0 mmol L^{-1}, respectively.

in the temperature range studied. In the presence of TFE at 25 °C these bands broaden and show shoulders on the high-energy side. Use of HFIP leads to more significant spectral changes, consistent with increased hydrogen bond donor strength. At room temperature the ν(CO) shows a shoulder at 1900 cm^{-1}, while the ν(OsH) broadens and shifts to high frequency, ν(OsH)$_{bonded}$ = 1964 cm^{-1}. As shown in Figure 7, the intensity of the ν(CO) of **1′** and the shift of the Os−H band from that at 25 °C both increase upon cooling to 200 K: ν(Os−H)$_{bonded}$ = 1967 cm^{-1} ($\Delta\nu_{1/2}$(OsH) = 34 cm^{-1}), ν(CO)$_{bonded}$ = 1900 cm^{-1}. The bands of the Os−H stretches are significantly broader than those of the C−O vibrations; their line widths in free **1** are 20 and 8 cm^{-1}, respectively. In contrast to the ν(CO), the ν(OsH) bands of **1** and **1′** are never resolved and only a composite of two broad, closely situated bands is observed. Apparently, however, the temperature changes shift equilibrium 1 and consequently alter the contribution of each ν(OsH) band to the observed one, which changes the intensity and maximum position of the single unresolved band.

The decrease in absorbance of the C−O stretching band of **1** in the presence of HFIP at several temperatures gave equilibrium constants *K*, which were analyzed to yield the thermodynamic parameters for the formation of the hydrogen bonded HFIP adduct **1′**. The values obtained from the van't Hoff plot, ΔH° = −3.7(5) kcal mol^{-1} and ΔS° = −9(1) cal mol^{-1} K^{-1}, agree satisfactorily with the enthalpy derived from the frequency shifts ($-\Delta H^\circ$ = 4.3(3) kcal mol^{-1}). In general, the latter method yields higher enthalpies, although the difference is within experimental error. Notably, the ΔS° derived from IR measurements in hexane is more negative than that determined by ^{1}H NMR in d_8-toluene (ΔS° = −6.6(5) cal mol^{-1} K^{-1}), consistent with "free" HFIP being hydrogen bonded to the aromatic ring of the latter solvent (*vide supra*).

(c) Structural Conclusions. Osmium complex **1** contains several potential hydrogen bond accepting sites: the oxygen atom of the carbonyl ligand, the hydride, the chloride, and the metal center. The described spectral changes in the range of 1700−2100 cm^{-1} indicate that neither the oxygen atom of the carbonyl ligand nor the hydride of **1** accept a hydrogen bond from HFIP, because low-frequency shifts of the corresponding bands are expected in such cases.[2a,k,6] These observations do not, however, discriminate between the chloride and the metal as the hydrogen bond acceptor. The IR region of 600−250 cm^{-1}, characteristic of the Os−Cl vibration, was therefore investigated and showed only one band, at 398 cm^{-1}, assigned to ν(OsCl). In the presence of HFIP, a low-frequency shoulder

(25) Iogansen, A. V. *Hydrogen Bond*; Nauka: Moscow, 1981; p 112.
(26) Epstein, L. M.; Krylov, A. N.; Shubina, E. S. *J. Organomet. Chem.* **1994**, *322*, 345.

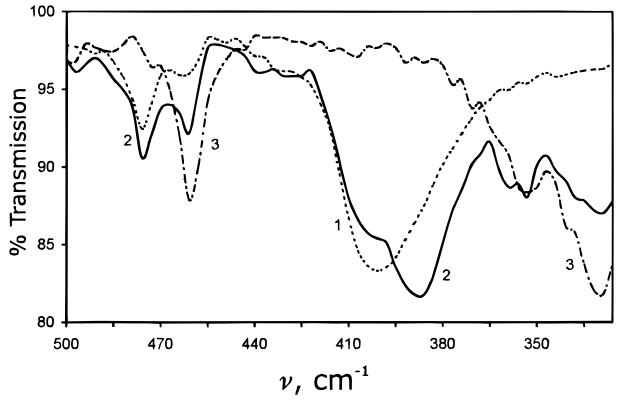

Figure 8. IR spectra of $OsHCl(CO)(P^tBu_2Me)_2$ (**1**)/HFIP (ν(OsCl) region, 20 °C) in hexane. The [**1**°]/[HFIP°] concentrations are 1.4/0 (**1**), 1.4/14 (**2**), and 0/24 (**3**) mmol L^{-1}, respectively.

at 378 cm^{-1} (Figure 8) was observed, consistent with participation of the chloride of **1** in the hydrogen bond with HFIP.

Despite the 16-electron nature of **1**, all IR observations indicate quite regular hydrogen bonding. The fluorinated alcohols donate hydrogen bonds to **1**, which involve the chloride ligand as the accepting site. No experimental data support significant O→Os coordination. The interactions formed in hexane are of moderate strength. The basicity factor of the accepting site in **1**, calculated according to[2k,27] Iogansen's "rule of factors" $E_j = -\Delta H_{ij}/(-\Delta H_{11}P_i)$ is 0.71 ($-\Delta H_{11} = 5.7$ kcal mol^{-1} for the standard pair PhOH/Et_2O in hexane; $P_i = 1.07$ is the acidity factor of HFIP), which is comparable, for example, with that of the nitrogen atom in *N*,*N*-dimethylamine ($E_j = 0.7$) and slightly greater than that in benzonitrile ($E_j = 0.68$).[27] It is interesting that the observed hydrogen-bonding interaction is significantly stronger than that with the chloride atom in haloalkanes (n-$C_7H_{15}Cl$[28] and n-$C_6H_{11}Cl$[29]) but weaker than that with the chloride ion.[30]

The non-fluorinated alcohols employed are weaker proton donors and therefore the IR spectral changes are expected to be less pronounced than those observed with the fluorinated analogs. On the other hand, the greater nucleophilicity of oxygen in MeOH and ^{i}PrOH allows one to anticipate stronger O→Os donation. Yet, the absence of changes in the O−H stretching region with MeOH and ^{i}PrOH and only slight changes in the region of C−O and Os−H vibration (shift of Os−H by 4−5 cm^{-1}) preclude any definite conclusions with regard to the O→Os coordination. The hydrogen bonding between **1** and HFIP was therefore investigated further through theoretical calculations.

III. Theoretical Studies. (a) Computational Models. We have used three different computational model systems to study the structure, energies, and vibrational frequencies of the adduct between the Os complex and an alcohol.

Model 1: $OsHCl(CO)(PH_3)_2$ (1^H) + CH_3OH is a simplified model without bulky substituents on ligands or alcohol. The hybrid density functional method B3LYP[31] was used with the LANL2DZ[32,33] basis set (called the basis set I (BS I)), a valence double-ζ set with a relativistic effective core potential for Os,[33a] Cl,[33b] and P[33b] centers.

Model 2: $OsHCl(CO)(PH_3)_2$ (1^H) + CF_2HOH is a model in which the more electron-withdrawing nature of the alcohol is represented with CF_2HOH. In addition to B3LYP/BS I, B3LYP/BS II was used to examine the effects of the basis set on the computed reults. Basis set II is an expansion of basis set I with a polarization shell on each of H(Os and O) (exponent 1.0), Cl (0.6), P (0.37), C(Os) (0.75), and O (0.85) atoms. The Os atomic basis is a 5d triple-ζ (541/321/111) contraction of the original basis set associated with the LANL2 relativistic effective core potential,[33a] and the C and F atoms of CF_2HOH are described with 6-31G(d)[34] and the PH_3 hydrogens with STO-3G.[35]

Model 3: $OsHCl(CO)(P^tBu_2Me)_2$ (1) + $(CF_3)_2CHOH$ is the real system for which the experiment has been carried out. This system was handled with the integrated MO + MM (IMOMM) method,[36−38] where the part corresponding to Model 2 was handled with the B3LYP/BS I method, while the remainder of the system, ^{t}Bu and Me groups of the P^tBu_2Me ligand, and the CF_3 groups of $(CF_3)_2CHOH$ were handled with the MM3 molecular mechanics force field[39] neglecting the electrostatic terms. Single-point calculations on the IMOMM-(B3LYP/BS I:MM3)-optimized geometries were also performed at the IMOMM(B3LYP/BS III:MM3) level of theory. Basis set III (BS III) was the same as BS II for the Os atom, while the rest of the system was described with the 6-311++G(d,p) basis set.[40] For details of the IMOMM method, see ref 36; specifics of our calculations are given in the Supporting Information. The analytical vibrational frequencies[41] for the MO fraction of the present system were calculated at the IMOMM optimized geometries by at first projecting out the MO Hessian matrix for the non-zero gradient component and then diagonalizing this projected Hessian matrix. These frequencies are reported here as those of the Model 3 system.

(27) (a) Iogansen, A. V. *Teor. Exp. Khim.* **1971**, *7*, 302. (b) Iogansen, A. V. *Teor. Exp. Khim.* **1971**, *7*, 312.
(28) Jones, D. A. K.; Watkinson, J. G. *J. Chem. Soc.* **1964**, 2366.
(29) West, R.; Powell, D. L.; Whatley, L. S.; Lee, M. K. T.; Schleyer, P. R. *J. Am. Chem. Soc.* **1962**, *84*, 3221.
(30) Epstein, L. M.; Saitkulova, L. N.; Shubina, E. S. *J. Mol. Struct.* **1992**, *270*, 325.
(31) (a) Becke, A. D. *J. Chem. Phys.* **1993**, *98*, 5648. (b) Lee, C.; Yang, W.; Parr, R. G. *Phys. Rev. B* **1988**, *37*, 785. (c) Stephens, P. J.; Devlin, F. J.; Chabalowski, C. F.; Frisch, M. J. *J. Phys. Chem.* **1994**, *98*, 11623.
(32) Frisch, M. J.; Trucks, G. W.; Schlegel, H. B.; Gill, P. M.; Johnson, B. G.; Wong, M. W.; Foresman, J. B.; Robb, M. A.; Head-Gordon, M.; Replogle, E. S.; Gomperts, R.; Andres, J. L.; Raghavachari, K.; Binkley, J. S.; Gonzalez, C.; Martin, R. L.; Fox, D. J.; Defrees, D. J.; Baker, J.; Stewart, J. J. P.; Pople, J. A. *Gaussian 92/DFT*; Gaussian Inc.: Pittsburgh, PA, 1993.
(33) (a) Hay, P. J.; Wadt, W. R. *J. Chem. Phys.* **1985**, *82*, 299. (b) Wadt, W. R.; Hay, P. J. *J. Chem. Phys.* **1985**, *82*, 284.
(34) (a) Ditchfield, R.; Hehre, W. J.; Pople, J. A. *J. Chem. Phys.* **1971**, *54*, 724. (b) Hehre, W. J.; Ditchfield, R.; Pople, J. A. *J. Chem. Phys.* **1972**, *56*, 2257. (c) Hariharan, P. C.; Pople, J. A. *Mol. Phys.* **1974**, *27*, 209. (d) Gordon, M. S. *Chem. Phys. Lett.* **1980**, *76*, 163. (e) Hariharan, P. C.; Pople, J. A. *Theor. Chim. Acta* **1973**, *28*, 213.
(35) (a) Hehre, W. J.; Stewart, R. F.; Pople, J. A. *J. Chem. Phys.* **1969**, *51*, 2657. (b) Collins, J. B.; Schleyer, P. v. R.; Binkley, J. S.; Pople, J. A. *J. Chem. Phys.* **1976**, *64*, 5142.
(36) Maseras, F.; Morokuma, K. *J. Comput. Chem.* **1995**, *16*, 1170.
(37) (a) Matsubara, T.; Maseras, F.; Koga, N.; Morokuma, K. *J. Phys. Chem.* **1996**, *100*, 2573. (b) Ujaque, G.; Maseras, F.; Lledos, A. *Theor. Chim. Acta* **1996**, *94*, 67. (c) Svensson, M.; Humbel, S.; Morokuma, K. *J. Chem. Phys.* **1996**, *105*, 3654. (d) Matsubara, T.; Sieber, S.; Morokuma, K. *Int. J. Quantum Chem.* **1996**, *60*, 1101. (e) Froese, R. D. J.; Morokuma, K. *Chem. Phys. Lett.* **1996**, *263*, 393. (f) Wakatsuki, Y.; Koga, N.; Werner, H.; Morokuma, K. *J. Am. Chem. Soc.* **1997**, *119*, 360. (g) Ogasawara, M.; Maseras, F.; Gallego-Planas, N.; Kawamura, K.; Ito, K.; Toyota, K.; Streib, W. E.; Komiya, S.; Eisenstein, O.; Caulton, K. G. *Organometallics* **1997**, *16*, 1979. (h) Barea, G.; Maseras, F.; Jean, Y.; Lledos, A. *Inorg. Chem.* **1996**, *35*, 6401. (i) Maseras, F.; Eisenstein, O. *New J. Chem.* **1998**, *22*, 5.
(38) Ujaque, G.; Maseras, F.; Eisenstein, O. *Theor. Chim. Acta* **1997**, *96*, 146.
(39) (a) Allinger, N. L. *mm3(92)*; QCPE: Bloomington IN, 1992. (b) Allinger, N. L.; Yuh, Y. H.; Lii, J. H. *J. Am. Chem. Soc.* **1989**, *111*, 8551. (c) Lii, J. H.; Allinger, N. L. *J. Am. Chem. Soc.* **1989**, *111*, 8566. (d) Lii, J. H.; Allinger, N. L. *J. Am. Chem. Soc.* **1989**, *111*, 8576.
(40) (a) Krishan, R.; Binkley, J. S.; Seeger, R.; Pople, J. A. *J. Chem. Phys.* **1980**, *72*, 650. (b) Frisch, M. J.; Pople, J. A.; Binkley, J. S. *J. Chem. Phys.* **1984**, *80*, 3265.
(41) Cui, Q.; Musaev, D. G.; Svensson, M.; Morokuma, K. *J. Phys. Chem.* **1996**, *100*, 10936.

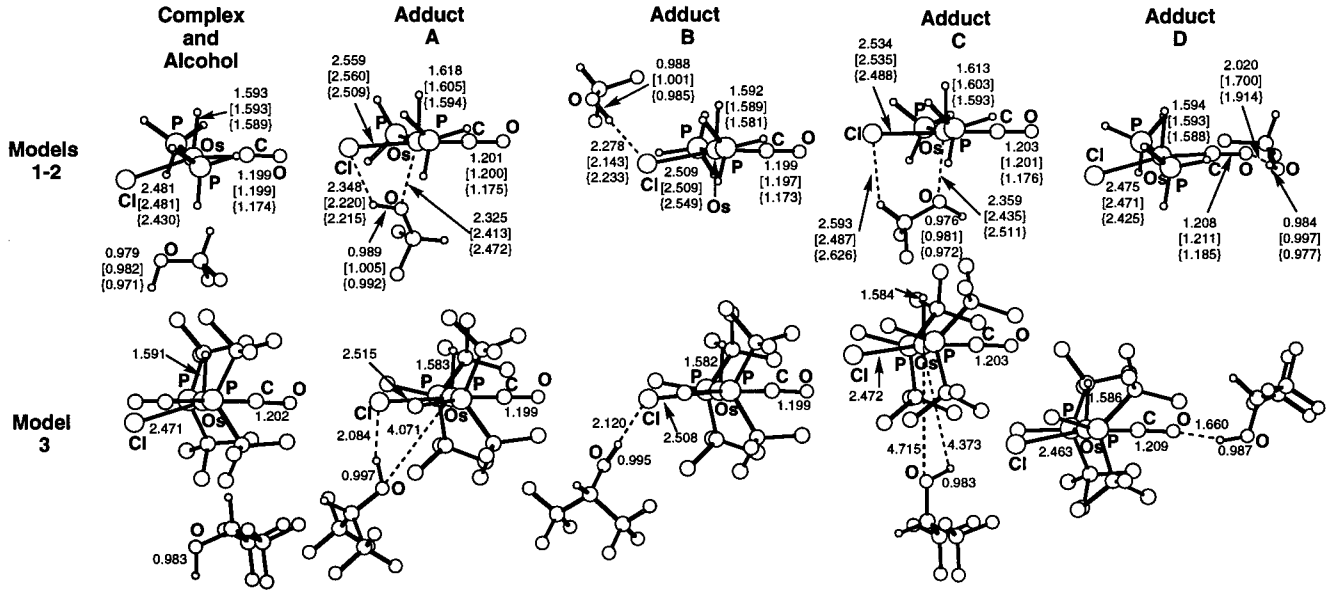

Figure 9. The geometries of the optimized structures with selected bond distances (Å). Distances for Models 1 and 3 are given in regular numbers, Model 2/BS I in square brackets, and Model2/BS II in curly brackets. Full Cartesian coordinates of all adducts, including **E**−**G**, may be found in the Supporting Information.

Optimization of the structures was done without symmetry constrains. The Cartesian coordinates of all optimized structures are given in the Supporting Information. The optimized adduct structures for Models 1 and 2 were confirmed to be real minima by the analytical Hessian matrix calculations.[41] Zero-point energy corrections (ZPCs) were obtained from the calculated harmonic frequencies without scaling. All calculations were performed with our own modification of the Gaussian92/DFT[32] and the Gaussian 94,[42] as well as with the development version[43] of the Gaussian 95.

(b) Optimized Structures for Models 1 and 2. Optimizations for Model 1 led to four adduct structures, **A**, **B**, **C**, and **D**, shown in Figure 9. Optimizations for Model 2 with BS I and BS II also gave essentially the same four structures, as also shown in Figure 9. In addition, structure **E** was found for Model 2 with both basis sets. Adducts **F** and **G** were found with Model 2/BS I and were not optimized with BS II or Model 1.

Structure **A** indicates a strong Os←O metal−ligand interaction, as well as a hydrogen-bonding interaction Cl···HO between the chloride ligand and the alcohol OH. The hydrogen bond is strongly bent, apparently due to the Os←O structural constraint, implying the OH group has to interact with the metal (more strongly) and the chloride (less strongly). As seen from Table 3, this structure is the global minimum for both Model 1 and Model 2 (both with BS I and BS II), with the binding energy of 17 kcal/mol for Model 1 and 11−13 kcal/mol for Model 2. The effects of the basis set are not very significant for both the geometrical parameters and energies. Structure **B** is a pure hydrogen-bond adduct (linear Cl···HO fragment), with no trace of the Os←O interaction. It is energetically much less stable than structure **A**, with the binding energy of 8−10 kcal/mol, regardless of Model and basis set.

Structure **C** indicates a strong (but slightly weaker than in **A**) Os←O interaction, supplemented with a Cl···HC hydrogen bond. The H atoms of CH groups in CH_3OH and CF_2HOH are significantly positively charged, so that the electrostatic Cl···HC interaction presumably takes place. This adduct is energetically about 3 kcal/mol less stable than the global minimum **A** for both Models 1 and 2. Adduct **D** exhibits a moderate (C)O···HO hydrogen bond. Structure **E**, found only for Model 2, is a pure Os←O metal−ligand adduct with no trace of hydrogen bonding interaction with Cl. This structure has a very small binding energy and has no physical significance. Adducts **F** and **G** are both based on Os···HO hydrogen bonding and are conformational isomers. Compared to adducts **A**−**D** (Table 3), weak binding energies of adducts **E**−**G** make them unlikely candidates for the experimentally observed adduct(s).

Models 1 and 2, which idealize the CF_3 and ^{t}Bu groups as H and/or F, may *artificially* allow for the existence of Os←O bonding. It is necessary to test this idea with a more complete representation of the CF_3 and ^{t}Bu groups.

(c) Optimized Structures for Model 3. Optimizations for Model 3, the real system experimentally studied, have been performed starting from the optimized structures of the adducts for Model 2. The results are shown also in Figure 9. Starting from **A** and **C**, optimization led to structures vastly different from the starting structures, but these still will be called **A** and **C**, respectively. Adducts **B** and **D** underwent relatively insignificant changes and retained their hydrogen-bonding patterns. Optimization from **E** resulted in dissociation of the adduct, while **F** and **G** both converged to adduct **D**.

The optimized structure **A** for Model 3 is essentially a pure hydrogen-bond adduct. Although the Os−O distance is shown in Figure 9, it is long (4.1 Å) and the interaction is completely

(42) Frisch, M. J.; Trucks, G. W.; Schlegel, H. B.; Gill, P. M. W.; Johnson, B. G.; Robb, M. A.; Cheeseman, J. R.; Keith, T.; Petersson, G. A.; Montgomery, J. A.; Raghavachari, K.; Al-Laham, M. A.; Zakrzewski, V. G.; Ortiz, J. V.; Foresman, J. B.; Cioslowski, J.; Stefanov, B. B.; Nanayakkara, A.; Challacombe, M.; Peng, C. Y.; Ayala, P. Y.; Chen, W.; Wong, M. W.; Andres, J. L.; Replogle, E. S.; Gomperts, R.; Martin, R. L.; Fox, D. J.; Binkley, J. S.; Defrees, D. J.; Baker, J.; Stewart, J. P.; Head-Gordon, M.; Gonzalez, C.; Pople, J. A. *Gaussian94, Revision A.1*; Gaussian, Inc.: Pittsburgh, PA, 1995.

(43) Frisch, M. J.; Trucks, G. W.; Schlegel, H. B.; Scuseria, G. E.; Robb, M. A.; Cheeseman, J. R.; Strain, M. C.; Burant, J. C.; Stratmann, R. E.; Dapprich, S.; Kudin, K. N.; Millam, J. M.; Livelsberger, A.; Petersson, G. A.; Montgomery, J. A.; Zakrzewski, V. G.; Raghavachari, K.; Ayala, P. Y.; Cui, Q.; Morokuma, K.; Ortiz, J. V.; Foresman, J. B.; Cioslowski, J.; Barone, V.; Stefanov, B. B.; Chen, W.; Wong, M. W.; Andres, J. L.; Replogle, E. S.; Gomperts, R.; Martin, R. L.; Fox, D. J.; Keith, T.; Al-Laham, M. A.; Nanayakkara, A.; Challacombe, M.; Peng, C. Y.; Stewart, J. P.; Gonzalez, C.; Head-Gordon, M.; Gill, P. M. W.; Johnson, B. G.; Pople, J. A. *Gaussian 95, Development Version (Revision F.1)*; Gaussian, Inc.: Pittsburgh, PA, 1996.

Table 3. The Binding Energies (in kcal/mol) of the Three Models of the Adducts Between the Os Complex and Alcohol[a]

adduct	contacts in Models 1 & 2	Model 1 B3LYP/BS I	Model 2 B3LYP/BS I	Model 2 B3LYP/BS II	Model 3 IMOMM (B3LYP/BS I:MM3)	Model 3 IMOMM (B3LYP/BS III:MM3)[b]
A	Os←O and Cl···HO	−19.19/−17.18	−14.24/−12.99	−12.12/−10.63	−7.90	−6.77
B	Cl···HO	−9.50/−8.38	−10.82/−10.12	−8.80/−7.89	−7.32	−6.26
C	Os←O and Cl···HC	−15.63/−13.71	−11.46/−10.23	−8.63/−7.25	−0.39	−0.27
D	(C)O···HO	−8.22/−6.99	−7.30/−6.59	−5.20/−4.34	−8.21	−4.56
E	Os←O	*c*	−0.88/+0.14	−3.19/−1.84	*c*	*c*
F	Os···HO	*d*	−1.57/−1.14	*d*	*c*	*c*
G	Os···HO	*d*	−3.90/−3.45	*d*	*c*	*c*

[a] The numbers before and after the slant are without and with ZPC, respectively. [b] Single-point calculations on Model 3 IMOMM (B3LYP/BS I:MM3) geometry. [c] Does not exist. [d] Not optimized.

Table 4. The Calculated Harmonic Frequencies (in cm^{-1}) for Models 1, 2, and 3 of the Os Complex and Alcohol before Adduct Formation and Their Shifts upon Adduct Formation for C−O, Os−H, Os−Cl, and Alcohol O−H Stretching, with the Corresponding Experimental Values

	Model 1 BS I				Model 2 BS I				Model 2 BS II				Model 3 BS I			
structure	C−O	Os−H	Os−Cl	O−H	C−O	Os−H	Os−Cl	O−H	C−O	Os−H	Os−Cl	O−H	C−O	Os−H	Os−Cl	O−H
1,**1**^{H} + alcohol	1901	2263	303	3704	1901	2263	303	3736	2017	2253	304	3813	1885	2268	303	3630
adduct **A**	−12	−86	−26	−189	−4	−34	−20	−473	−3	−10	−19	−400	+14	+20	−25	−295
adduct **B**	0	+3	−21	−168	+7	+9	−21	−417	+4	+49	−17	−268	+13	+20	−19	−259
adduct **C**	−22	−70	−21	+53	−10	−39	−23	−40	−10	0	−19	−6	−5	+10	0	+48
adduct **D**	−45	−3	−1	−80	−51	0	+7	−360	−109	+15	+2	−120	−22	+15	+8	−100
adduct **E**	*a*				−28	−11	−10	−43	−21	+24	−8	+7	*a*			
adduct **F**	*b*				−22	−12	+10	−159	*b*				*a*			
adduct **G**	*b*				+3	−5	+9	−294	*b*				*a*			
1 or alcohol (exper)													1889	1948	398	3611
adduct (exper)													+11	+16	−20	−233

[a] Does not exist. [b] Not optimized.

lost. Now that the metal−ligand Os←O interaction is lost, the Cl···HO interaction is not subject to structural constraint and becomes linear. A significant decrease of the MM contribution to the integrated MO+MM energy during the optimization process indicates that the steric or exchange repulsion between the ^{t}Bu substituent on the phosphine and the alcohol prevents the alcohol from penetrating the vicinity of the Os center. Since the Cl hydrogen bond site is located far away from the bulky ^{t}Bu substituents, the approach of the OH group to Cl is not sterically hindered. One notices that the binding energy for Model 3, about 8 kcal/mol without ZPC, is 12 and 6 kcal/mol smaller than those for structure **A** of Models 1 and 2. In structure **A** of Model 3, compared to those of Models 1 and 2, the Os←O metal−ligand interaction has been lost and the Cl···HO hydrogen bond has been strengthened by linearizing its structure.

The newly optimized structure **B** for Model 3, with a linear Cl···HO hydrogen bond local structure, is very similar to structure **A** just discussed. As shown in Table 3, these two adducts are energetically very similar as well. We suspect that there exist many local minima of similar structures, with different orientations of the alcohol and different conformations of substituted phosphines. These structures are expected to be similar in energy, geometrical parameters, and molecular properties such as vibrational frequencies.

Structure **C**, without hydrogen bond or metal−ligand interaction, is only slightly bound without ZPC; we expect the structure to be unbound with ZPC, and therefore to have no physical significance.

Structure **D** with the (C)O···HO hydrogen bond is the most stable according to the Model 3 BS I level. Compared to the MO calculations on the model system, structure **D** is even more stabilized upon introduction of the steric effects. Favorable both sterically and electronically, stronger Os−Cl interaction, reflected in shortening of the Os−Cl distance, is believed to be the reason for this stabilization.

Summarizing, the steric effects assessed with IMOMM calculations on the real system hinder the formation of the Os←O bond, which agrees with the conclusions drawn from experimental data. Two hydrogen bond accepting sites are found with our calculations: Cl and O atoms of **1**.

Concerning the hydrogen-bonding studies, density functional theories are known to be very sensitive to the basis set,[44a−f] and gradient corrected functionals with *extensive* basis sets containing diffuse functions are needed for a reliable description of hydrogen bonds.[44g−i] Therefore, we have performed single-point calculations at the IMOMM(B3LYP/BS III:MM3) level. In this calculation, structure **D** becomes less stable than **A** and **B** (Table 3).

Since the energetics alone may not be very reliable, we analyzed vibrational frequencies of various adducts to determine which structure(s) satisfies the experimental observations.

(d) Vibrational Frequencies. As clear points of comparison with experiment, the shifts, reported here, of vibrational frequencies upon adduct formation for the C−O, Os−H, Os−Cl stretch normal modes of the metal complex, as well as the O−H stretch normal mode of the alcohol, were all calculated. These, relative to those of the complex and alcohol before adduct formation, are shown in Table 4 and compared with the experimental values. In Models 1 and 2, only structure **B**, with the Cl···HO hydrogen bond but without Os←O interaction, crudely follows the experimental pattern of shifts. However, the agreement is rather poor and structure **B** is much less stable than structure **A** in both Models 1 and 2 (Table 3). On the

(44) (a) Csonka, G. I.; Ahn, N.; Angyan, J.; Csizmadia, I. G. *Chem. Phys. Lett.* **1995**, *245*, 129. (b) Topol, I. A.; Burt, S. K.; Rashin, A. A. *Chem. Phys. Lett.* **1995**, *247*, 112. (c) Bohr, Y. J.; Ruiz-Lopez, M. F. *Can. J. Chem.* **1995**, *73*, 710. (d) Florian, J.; Johnson, B. G. *J. Phys. Chem.* **1995**, *99*, 5899. (e) Novoa, J. J.; Sosa, C. *J. Phys. Chem.* **1995**, *99*, 15837. (f) Han, W.-G.; Suhai, S. *J. Phys. Chem.* **1996**, *100*, 3942. (g) Kang, H. C. *Chem. Phys. Lett.* **1996**, *254*, 135. (h) Jeong, H. Y.; Han, Y.-K. *Chem. Phys. Lett.* **1996**, *263*, 345. (i) Zhang, Q.; Bell, R.; Truong, T. N. *J. Phys. Chem.* **1995**, *99*, 592.

other hand, for Model 3, both structures **A** and **B**, having nearly the same mode of interaction, linear Cl···HO hydrogen bonding with no Os←O, and similar energy, give the pattern of vibrational frequency shifts which nearly quantitatively agree with the experiment.

At the same time, with all Models, vibrational frequency shifts for adduct **D** are in crucial contradiction with the experiment. An enormous *low-frequency* C−O shift calculated for adduct **D** disagrees with the experimentally observed *high-frequency* shift.

We therefore conclude, based both on the BS III energetics and the vibrational analysis, that OH···Cl bond is more stable than (C)O···HO, and that the actual adduct is bound through the OH···Cl hydrogen bond (as in adducts **A** and **B**).

Discussion

The results presented above provide unambiguous evidence for the formation of a 1:1 adduct between **1** and HFIP in solution, bound exclusively via an (O)H···Cl(Os) hydrogen bond. The "push−pull" stabilization[45] of the formally unsaturated **1**, partly delocalizing the π-density of the chloride into the π^* orbitals of the carbonyl ligand, nevertheless leaves the former the most nucleophilic site of the osmium complex. Although similar hydrogen bonding was observed between the *fluoride* ligand of RuHF(CO)(P^{t}Bu$_2$Me)$_2$ and weakly Brønsted acidic electrophiles,[14b,c] the reactivity of such π-stabilized five-coordinate compounds[14b] toward conventional hydrogen-bond donors (e.g., H_2O, ROH) is not well studied. Since hydrogen bonding is known to polarize the A−H donor group in the $A^{\delta-}$−$H^{\delta+}$ sense,[46] it promotes coordination of the heteroatom (**A**) to an unsaturated metal center. Coordination of Me<u>O</u>H and H_2<u>O</u> to $OsH_3Cl(P^iPr_3)_2$[47] and $[OsHCl(NO)(P^iPr_3)_2^+]$,[48] respectively, may be assisted by (O)H···Cl(Os) hydrogen bonding, while such bifunctional coordination of phenylacetylene was proposed to mediate the exchange of fluoride and alkoxides for phenylacetylide in RuHX(CO)(P^{t}Bu$_2$Me)$_2$ (X = F, OR).[14b] The crucial feature of the hydrogen-bonding pattern firmly established here lies in the increased unsaturation at the metal center unaccompanied by coordination of the alcohol oxygen. The calculations outline the effect of the hydrogen bonding on the electronic structure of **1** and provide an insight into the interplay of steric and electronic factors responsible for the adduct geometry.

(a) Electronics of the Hydrogen Bonding. As the most appropriate static model for experimentally observed adduct **1′** (Table 4), calculated adduct **B**/Model 3 contains an (O)H··· Cl(O) hydrogen bond as the only conceivable **1**-HFIP interaction (Figure 9). The H···Cl distance of 2.120 Å falls well within the OH···Cl$^-$ range of [2.02−2.43] Å, observed for moderate hydrogen bonds in crystal structures of nucleic acid components.[49] The hydrogen bond is essentially linear (∠O−H···Cl 177.9°) and shows some directionality with respect to the Os−Cl bond (∠H···Cl−Os 119.8°, dihedral ∠H···Cl−Os−H 145.2°). The Kitaura−Morokuma energy decomposition analysis,[50] applied at the Hartree−Fock level to the MO part of IMOMM-optimized adduct **B**, $\{\mathbf{1^H}\}_{\mathbf{B3}}$, is presented in Table 5. The main attractive component (72%) is the electrostatic (ES) interaction.

Table 5. The Kitaura−Morokuma Energy Decomposition Analysis[50] of the Hydrogen Bond Interaction Energy in Adduct **B**/Model 3[a]

	E	ES	EX	PL	CT	MIX
total	−12.02	−15.34	9.26	−1.88[b]	−3.72	−0.34
$\{\mathbf{1^H}\}_{\mathbf{B3}} \rightarrow \{CF_2HOH\}_{\mathbf{B3}}$[c]				−0.35	−3.26	
$\{CF_2HOH\}_{\mathbf{B3}} \rightarrow \{\mathbf{1^H}\}_{\mathbf{B3}}$[d]				−1.36	−0.46	

[a] In kcal mol^{-1} for the MO part $\{\mathbf{1^H}+CF_2HOH\}_{\mathbf{B3}}$ at the Hartree−Fock level. [b] Includes high-order coupling of the two components. [c] CT from $\{\mathbf{1^H}\}_{\mathbf{B3}}$ to $\{CF_2HOH\}_{\mathbf{B3}}$, PL of $\{CF_2HOH\}_{\mathbf{B3}}$ by $\{\mathbf{1^H}\}_{\mathbf{B3}}$. [d] CT from $\{CF_2HOH\}_{\mathbf{B3}}$ to $\{\mathbf{1^H}\}_{\mathbf{B3}}$, PL of $\{\mathbf{1^H}\}_{\mathbf{B3}}$ by $\{CF_2HOH\}_{\mathbf{B3}}$.

A small but significant (17%) contribution comes from the charge transfer (CT), mainly from the metal complex to the alcohol, while the polarization (PL) contributes the least (9%) and is predominantly due to the polarization of $\mathbf{1^H}$ by CF_2HOH. All these features characterize the (O)H···Cl(Os) hydrogen bond in adduct **B**/Model 3 as quite regular,[50c,e] consistent with the small experimental enthalpy of formation of **1′**.

Shown in Figure 10 are the spatial representations of the canonical valence molecular orbitals of $\mathbf{1^H}$ (Model 2/BS I).[51b] The "push−pull" interactions are clearly reflected in the OC−Os in-phase mixing of the two orthogonal CO π^* orbitals with both bonding and antibonding combinations of the filled Os d_π and Cl p_π orbitals, alleviating their repulsion.[45,52] Preference of the hydrogen bonding to the chloride is not surprising, as the top five filled orbitals contain significant chloride p_π character.

Figure 11 shows MO energy diagrams for the formation of H···Cl adducts **B** with both Model 2 (BS I) and Model 3[53] calculations. The (O)H···Cl(Os) hydrogen bond results in stabilization of all the valence molecular orbitals of the metal complex, including the vacant ones. These energy changes indicate that the hydrogen bond acceptor becomes electron deficient and more unsaturated, taking the LUMO energy as a crude estimate. Although no decomposition analysis was performed for the MO energies, it is noted that in a similar strongly electrostatic $(H_2O)_2$ hydrogen bonded C_s dimer[50e] analogous stabilization of the acceptor orbitals was found to be essentially determined by electrostatic interactions.[50c] Since the nominal characters of the $\mathbf{1^H}$ MO's is largely retained in the H···Cl complexes (i.e., the mixing with the MO's of CF_2HOH is small), it is notable that the Cl p_z orbital undergoes significantly greater stabilization than does the Cl p_x orbital, consistent with the hydrogen bond directionality mentioned above.

Structurally, the (O)H···Cl(Os) hydrogen bond diminishes the "push−pull" Cl→Os→CO π interactions. This is most clearly reflected in the weakening of the Os−Cl bond (+0.037 Å Δ-(Os−Cl), −19 cm^{-1} $\Delta\nu$(Os−Cl)) and the corresponding strength-

(45) Caulton, K. G. *New J. Chem.* **1994**, *18*, 25.

(46) Kollman, P. A. *Applications of Electronic Structure Theory*; Schaefer, H. F., III, Ed.; Plenum Press: New York, 1977; Vol. 3, Chapter 3.

(47) Kuhlman, R.; Clot, E.; Leforestier, C.; Streib, W. E.; Eisenstein, O.; Caulton, K. G. *J. Am. Chem. Soc.* **1997**, *119*, 10153.

(48) Yandulov, D. V.; Streib, W. E.; Caulton, K. G. *Inorg. Chim. Acta* **1998**, *280*, 125.

(49) Jeffrey, G. A. *An Introduction to Hydrogen Bonding*; Oxford University Press: New York, 1997.

(50) (a) The Kitaura−Morokuma energy decomposition analysis[50b] has been widely and successfully used in analyses of a number of hydrogen bonded complexes.[50c−e] The following partitioning of the interaction energy ($E = E_{\text{"complex"}} - E_{\text{"monomers"}}$ {at the geometries adopted in the "complex"}) is possible: E = ES + PL + EX + CT + MIX, where ES is the electrostatic interaction, PL is the polarization, EX is the exchange repulsion, CT is the charge-transfer, and MIX is the coupling term between the other four. See ref 50c for more details. (b) Kitaura, K.; Morokuma, K. *Int. J. Quantum Chem.* **1976**, *10*, 325. (c) Umeyama, H.; Morokuma, K. *J. Am. Chem. Soc.* **1977**, *99*, 1316. (d) Umeyama, H.; Morokuma, K. *J. Am. Chem. Soc.* **1976**, *98*, 4400. (e) Morokuma, K. *Acc. Chem. Res.* **1977**, *10*, 294.

(51) (a) Molden 3.2. Copyright 1991, Cijs Schaftenaar. (b) Those corresponding to the MO part of the optimized **1**/Model 3, $\{\mathbf{1^H}\}_{\mathbf{1}}$, are essentially the same in character; however, Os d_{xy} and d_{yz} are accidentally degenerate.

(52) Heyn, R. H.; MacGregor, S. A.; Nadasdi, T. T.; Ogasawara, M.; Eisenstein, O.; Caulton, K. G. *Inorg. Chim. Acta* **1997**, *259*, 5.

(53) The MO parts of the IMOMM calculations are used: $\{\mathbf{1^H}\}_{\mathbf{1}}$ and $\{\mathbf{1^H}+CF_2HOH\}_{\mathbf{B3}}$.

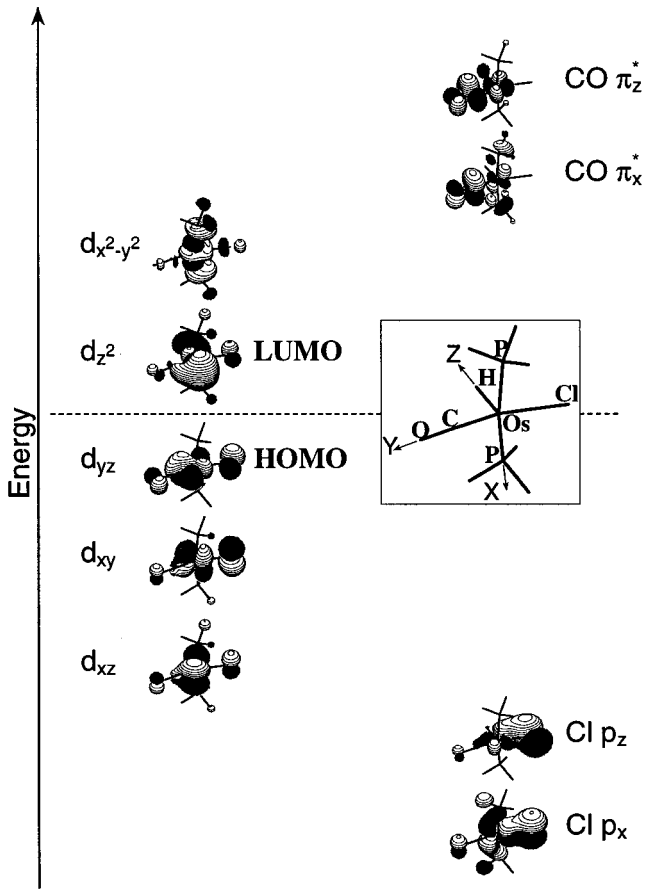

Figure 10. Spatial representations[51a] of the canonical valence MO's of $OsHCl(CO)(PH_3)_2$ ($\mathbf{1^H}$) computed with Model 2, BS I. The labels indicate the nominal characters.

ening of the carbonyl C−O bond (−0.003 Å Δ(C−O), +13 cm^{-1} Δν(CO)) in adduct **B**/Model 3. Such effect is likely to be due to the polarization (PL) component of the hydrogen bonding (Table 5), which is known to be the largest contributor to the charge redistribution in regular hydrogen bonded complexes,[50c] with some additional $\mathbf{1^H}$→CF_2HOH charge transfer (CT) contribution. The electrophilic O−H group polarizes the electron distribution of the metal complex in the $Cl^{\delta-}$−$Os^{\delta+}$ sense, giving rise to an attractive interaction with thereby induced multipoles.[50d] Together with CT, PL may contribute to the lowering of the LUMO in energy in $\mathbf{1^H}$ (Figure 11). The electron-withdrawing influence such polarization has on the metal complex is evident in the strengthening of the Os−H bond (−0.009 Å Δ(Os−H), +20 cm^{-1} Δν(Os−H)), consistent with increasing σ-stabilization of the metal,[52] and lengthening of the Os−P bond by ≥0.008 Å, which agrees with the metal becoming a harder Lewis acid.[54] Accordingly, the Mulliken charge on Os decreases by 0.065 e, while that on Cl increases by 0.031 e upon formation of the hydrogen bond.

Summarizing, these criteria show that the (O)H···Cl(Os) hydrogen bonding increases the unsaturation of osmium in **1′**, which should promote ligand binding at the sixth coordination site.

However, just as the hydrogen bonding increases the electrophilicity of the osmium, the alcohol oxygen becomes more nucleophilic. Simultaneous O→Os coordination is thus stimulated and is evident already in adduct **A**/Model 3, providing an extra 0.6 kcal mol^{-1} binding energy, compared to **B**. The

(54) Orpen, A. G.; Brammer, L.; Allen, F. H.; Kennard, O.; Watson, D. G.; Taylor, R. *J. Chem. Soc., Dalton Trans.* **1989**, S1.

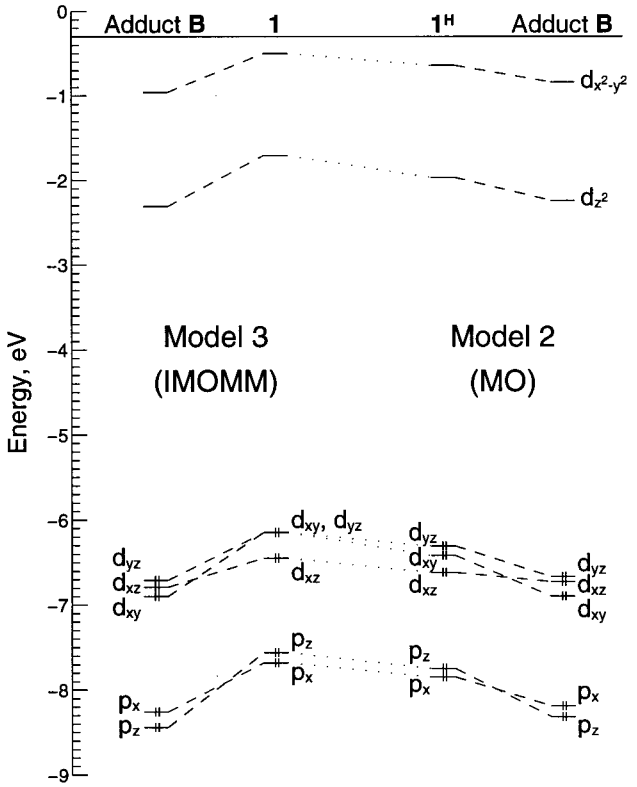

Figure 11. Effect of the (O)H···Cl(Os) hydrogen bonding on the MO energy levels of **1**.

decrease of Os···O from 4.870 Å in adduct **B** to 4.072 Å in **A** is accompanied by shortening of the H···Cl bond by 0.036 Å, bending of the hydrogen bond (−11.6° Δ∠O−H···Cl, −22.5° Δ∠O−H···Cl−Os), and weakening of the Os−Cl (+0.007 Å Δ(Os−Cl), −6 cm^{-1} Δν(Os−Cl)) and O−H (+0.002 Å Δ(O−H), −36 cm^{-1} Δν(O−H)) bonds. Considering the very long (4.071 Å) Os···O distance, the interaction in adduct **A**/Model 3 is clearly electrostatic and virtually nonexistent. Electronically, however, such simultaneous [Os←O + H···Cl] binding of the alcohol is highly favored, as adduct **A**/Model 2 (BS I) has a much larger binding energy than that of **B**/Model 3. The shortest Os−O and the longest Os−Cl bond distances found in the former adduct out of all the CF_2HOH adducts considered indicate the cooperative nature of the H···Cl and O→Os electron donor−acceptor interactions.[50e] Such cooperativity is well-known for hydrogen bonding in organic systems,[49] with clear partitioning into resonance-assisted (π-electrons) and polarization-enhanced (σ-electrons) types. These findings in our case suggest a possibility of further enhancement of ligand binding by the metal in **1′** through analogous [L→Os + (RO)-H···Cl(Os)] cooperativity as well as its importance in reactivity of **1** with Brønsted acidic substrates.[14b]

(b) Influence of Steric Factors. The steric bulk preserves the sixth coordination site in **1′** unoccupied simultaneously with hydrogen bonding, providing the difference *E*(**A**/Model 3) − *E*(**A**/Model 2 (BS I)) of about 6 kcal mol^{-1} to cooperative [Os←O + H···Cl] binding of HFIP. The influence of the bulky P^tBu_2Me phosphines already in free **1**, evident in hindered rotation about the Os−P bonds, is also noticeable in the calculations. The IMOMM-optimized structure has the Os−Cl bond shorter than that in $\mathbf{1^H}$ by 0.01 Å, and Os−P distances longer by 0.05 Å. The repulsion of the chloride ligand with the phosphines is responsible for the Os−Cl shortening, because MO optimization of the $\{\mathbf{1^H}\}_1$ with fixed Os−P distances led to the same Os−Cl bond length as in fully MO-optimized $\mathbf{1^H}$.

Notably, such shortening improves the calculated ν(CO) value (Table 4) by increasing the extent of "push−pull" interactions. Figure 11 shows that such distortion destabilizes all the valence orbitals of $\mathbf{1^H}$, formally increasing the nucleophilicity of the chloride ligand.

Conclusions

Theoretical calculations indicate that the simplified model complex + alcohol without bulky substituents is not even a qualitatively acceptable model for the experimentally studied adduct. Only Model 3, the real complex and real alcohol with bulky substituents, treated with the IMOMM method, removes sterically-hindered Os←O interaction. Comparison of the computed frequency shifts with the experimental results suggests the Cl···HO linear hydrogen bond structure (without metal−ligand interaction) of the adduct. We note that the actual adduct observed may be a dynamic statistical average of different structures, with the common element of the OH···Cl hydrogen bond. Two adducts (**A** and **B**) were shown to be the most stable at the IMOMM(B3LYP/BS III:MM3) level and the most sophisticated level of theory used in the present paper and to reproduce reasonably well the experimentally observed vibrational frequency shifts.

The structure of the experimentally studied adduct is dictated by the steric repulsion between the bulky substituents on phosphines and the alcohol, which precludes the intrinsically preferred Os←O interaction, leaving only the Cl···HO hydrogen bond, which can be formed outside the sterically-congested region.

Such hydrogen bonding in OsHCl(CO)(P^tBu_2Me)$_2$ increases unsaturation at the metal center. While simultaneous coordination of the alcohol oxygen to the vacant site would be enhanced by the hydrogen bonding, the steric bulk of the phosphines effectively protects the metal center. The possible applications of such interaction include moderating the reactivity at a broad range of analogous unsaturated metal centers via conceptually simple and convenient homogeneous electrophilic additives. Knowledge of the hydrogen bond type interrogated here, on the other hand, may assist in providing mechanistic insights into the reactivity of Brønsted acidic substrates with unsaturated compounds containing π-donor ligands.

Experimental Section

NMR Experiments. Complex OsHCl(CO)(P^tBu_2Me)$_2$ (**1**) was prepared by a published procedure[13a] and additionally recrystallized prior to the set of measurements.[55] Traces of crystallization solvent (1,2-dimethoxyethane) were removed by dissolving the compound in ether and evaporating the solution. HFIP was purchased from Aldrich and dried over molecular sieves. Toluene-d_8 was dried over sodium metal, vacuum distilled, freeze−pump−thaw degassed five times, and stored in an argon-filled glovebox. NMR samples were prepared by the following typical procedure: a solution of 3 μL of HFIP in 0.5 mL of d_8-toluene prepared in an argon-filled glovebox is placed in an NMR tube fitted with a Teflon stopcock and vacuum-transferred into a regular 5 mm NMR tube containing the appropriate amount of OsHCl(CO)(P^tBu_2Me)$_2$, also weighed in the glovebox, followed by sealing of the tube under vacuum. ^{1}H and ^{31}P NMR spectra were run on a Varian Gemini 2000 spectrometer (^{1}H: 300 MHz; ^{31}P: 122 MHz) and referenced to the residual protio solvent peaks (^{1}H) or external 85% H_3PO_4 (^{31}P). Temperatures from ambient to −100 °C were calibrated with a methanol standard. All samples were allowed at least 10 min to equilibrate at every temperature, which was maintained to ±0.5°. Standard Varian software was used for the inversion−recovery T_1 and NOE measurements. All numerical data manipulation and plotting was done with Matlab 5.0.[56] Standard error propagation formulae[57] were used in the error analysis of the obtained values of $\Delta H°$ and $\Delta S°$. Although the relative errors in the values of the equilibrium constants (Table 2) are within 2%, 10% uncertainty was assumed for the constants and 1° for the temperatures in order to partially account for neglected possible correlation of errors between the two. Solubility limitations of the metal complex restricted the NMR studies to d_8-toluene as the least polar solvent, while $(CF_3)_2CHOH$ (HFIP) was found to be sufficiently acidic ($pK_a = 9.2$) to result in an observable interaction. Different [**1**°] to [HFIP°] ratios were achieved by varying the concentration[58] of **1** from 11.4 to 114 mmol L^{-1}, with [HFIP°] kept constant at 57.0 mmol L^{-1} to avoid self-association.

IR Experiments. IR spectra were recorded on a Specord-M82 spectrometer in CaF_2 cells (d = 0.12−2.2 cm). Polyethylene cells (d = 0.4 mm) were used for low-frequency regions. All experiments were carried out in hexane, which was distilled in an atmosphere of dry, oxygen-free argon and degassed prior to every set of measurements. Concentrations of alcohols were varied from 1.0 to 14.0 mmol L^{-1} to exclude self-association. The region of O−H stretching vibrations of the alcohols used was investigated at [**1**°]/[ROH°] mole ratios from 1 to 5 ([ROH°] = 1.0 mmol L^{-1}, [**1**°] varied from 1.0 to 5.0 mmol L^{-1}), while 1- to 10-fold molar excess of the alcohols ([**1**°] = 1.0, 1.4 mmol L^{-1}, [ROH°] varied from 1.0 to 14.0 mmol L^{-1}) was employed in analyzing ligand vibrations of **1**. Solutions were prepared with use of standard Schlenk techniques and transferred into the IR cell in a counterflow of argon. Cold solutions were similarly transferred into the precooled cell (CaF_2 d = 1.2 mm or polyethylene d = 0.4 mm) of the cryostat in the low-temperature experiments, which were run from 190 to 300 K. Temperature was measured with 0.5 K error. Equilibrium constants for formation of **1′** (see text) were measured by a decrease in absorbance of the C−O stretching band of **1** with the necessary assumption of insignificant interference from the partially overlapping C−O band of **1′**.

Acknowledgment. This work was supported by the U.S. National Science Foundation. We also thank the Russian Foundation for Basic Research (Grant 96-03-34114). D.V.K. and K.M. deeply thank the authors of the IMOMM, and its current methodology, in particular Dr. Feliu Maseras for helpful discussions and valuable preprints.

Supporting Information Available: Details of the IMOMM calculations and Cartesian coordinates of all optimized structures (8 pages, print/PDF). See any current masthead page for ordering information and Web access instructions.

JA980751P

(55) The deuterio analog of **1** was found to exchange Os−D with the phosphine protons in the solid state on the time scale of months.

(56) Copyright 1984−96, The Math Works, Inc., Version 5.0.0.4064.

(57) Bevington, P. R. *Data Reduction and Error Analysis for the Physical Sciences*; McGraw-Hill Book Company: New York, 1969; Chapter 4.

(58) OsHCl(CO)(P^iPr_3)$_2$ was shown to be monomeric in benzene by osmometry, see ref 13b.